Collective and single-particle excitations in liquid neon

W. J. L. Buyers and V. F. Sears
Atomic Energy of Canada Limited, Chalk River Nuclear Laboratories, Chalk River, Ontario, Canada K0J 1J0

P. A. Lonngi and D. A. Lonngi*
Instituto Nacional de Energia Nuclear, Mexico, D.F., Mexico
(Received 19 August 1974)

The neutron inelastic scattering from orthobaric liquid neon at 26.9 °K has been measured with a triple-axis crystal spectrometer operating in its constant-Q mode. The scattering was measured as a function of frequency ν for 34 values of Q in the range 0.8–12.5 Å^{-1}. Corrections for residual multiple scattering and instrumental resolution were applied to the theoretical cross sections before comparing with experiment. In the *region of collective behavior*, $Q \lesssim 4$ Å^{-1}, the quasielastic peak that is observed is in qualitative agreement with the Kerr-Singwi theory and with the memory-function theory, which is applied to neon in the present work. The observed scattering at constant Q (<1.6 Å^{-1}) shows a pronounced inelastic wing at values of ν where the memory-function theory predicts a small inelastic peak. No such wing is contained in the Kerr-Singwi theory. The latter theory evidently overestimates the damping of the collective motion while the former underestimates it. The observed scattering in the region $Q>4$ Å^{-1} is characteristic of *single-particle scattering*. The peak position follows, but lies somewhat lower than, the recoil frequency $\hbar Q^2/4\pi m$, where m is the mass of a neon atom, and the width of the scattering function increases approximately linearly with Q. Superimposed on this general behavior are well-defined oscillations characteristic of the coherent nature of the scattering. The single-particle scattering in liquid neon is very similar to that observed in liquid helium. The data in the single-particle region are in reasonable agreement with the Kerr-Singwi model and in even better agreement with a truncated Gram-Charlier expansion. The earlier data of Chen *et al.* are corrected for the nonlinearity inherent in a time-of-flight experiment and are found to agree with the present results in showing that there are no well-defined propagating excitations in liquid neon for $Q \geqslant 0.8$ Å^{-1}.

I. INTRODUCTION

In the past 15 years the study of phonons in crystals by coherent neutron inelastic scattering has led to a very detailed understanding of the motion of atoms in solids and of the interatomic forces which produce this motion. The situation with regard to liquids is quite different because one is dealing with a medium which is both spatially disordered and highly anharmonic. Also, apart from liquid helium, the liquid is a thermodynamic state far removed from the ground state, so that there is no longer the simplification which occurs in crystals at low temperatures from the fact that the system is dynamically equivalent to a dilute gas of weakly interacting phonons. As a result, the neutron inelastic scattering in a liquid—and particularly in a classical monatomic liquid—tends to be rather featureless, as far as its dependence on frequency transfer is concerned, consisting predominantly of a single broad peak with little if any structure in the wings. Hence the neutron data are difficult to interpret without the help of a detailed theory of the entire scattering cross section.

In the past few years the development of, for example, memory-function techniques and asymptotic expansions for large wave-vector transfer provides nontrivial means for interpreting the data. In addition, the quality of the data themselves has improved with the development of techniques for reducing and/or correcting for effects of multiple scattering. A case in point is the recent very beautiful work of Sköld and co-workers on liquid argon.[1,2]

One can list three basic types of information which may be obtained from coherent inelastic scattering in monatomic liquids: (i) the way in which the hydrodynamic (first-sound) regime at small values of the wave-vector transfer Q goes over at intermediate values of Q to a collective regime which, in crystals, would be called the zero-sound or phonon regime; (ii) the nature of the atomic motion in the collective regime; (iii) the way in which the collective regime goes over to the single-particle regime at large Q. In many respects liquid neon is ideally suited to studying these problems. It is intermediate in the Periodic Table between helium, in which the collective motion in the liquid produces well-defined phonon peaks in the neutron data,[3,4] and argon, in which it does not. Thus, for example, if the concept of a zero-sound mode has any relevance at all for classical liquids it should certainly apply to neon. Neon (unlike argon) is an almost totally coherent scatterer,[5] so that it is unnecessary to correct the data for incoherent scattering. The atomic mass

of neon is small enough that the transition from the collective regime to the single-particle regime occurs in a region of Q values which is easily accessible to available experimental techniques. Finally, the interatomic forces in liquid neon are known[6] with sufficient accuracy that a direct comparison of theory and experiment can be made without any adjustment of parameters. For these reasons we have undertaken the detailed investigation of neutron-inelastic scattering in liquid neon, which we now describe.[7]

II. EXPERIMENT

A. Specimen

The neon was research grade (99.995%) with helium content less than 50 ppm and hydrogen less than 5 ppm. The gas was condensed into a vertical cylindrical aluminum cassette of diameter 0.5 in., length greater than the 2-in. beam height, and wall thickness 0.010 in. The transmission of the sample was 92%. Multiple scattering was further reduced by hanging from a wire a set of parallel 0.002-in.-thick stainless-steel disks spaced 0.1 in. along the cylinder axis. The wire and discs were plated with a 0.002-in. layer of cadmium on all surfaces. The residual multiple scattering can be calculated accurately for such a configuration and is found in Sec. III to be small, typically 2% at large Q.

The temperature of the neon was held at 26.90 ± 0.15 °K by means of a temperature controller and platinum resistance thermometer. The platinum thermometer was calibrated against the more accurate temperature given by the vapor pressure of the neon.

B. Neutron spectroscopy

The scattering function[8] $S(Q, \nu)$ was obtained from measurements made with the triple-axis crystal spectrometer at the C5 facility of the NRU reactor at Chalk River. The spectrometer was operated at constant wave-vector transfer Q, with variable incident energy E_0. This method of measuring $S(Q, \nu)$ is free (see Sec. V E) of the λ^4 sensitivity factor and the variation of detector efficiency that distort observed peak shapes in time-of-flight work or triple-axis measurements with variable scattered energy E. Higher-order contaminants in the beam were reduced to negligible proportions by use of a Ge monochromator.[9]

Steel segments 20 in. long placed along either side of the incident-beam collimator limited the beam width to 1 in. in order to reduce background. Since a large range of wave-vector transfers was studied, $0.8 \leq Q \leq 12.5$ Å^{-1}, it was necessary to optimize the resolution for three different ranges of wave-vector transfer. The corresponding monochromator-analyzer combinations are given in Table I and the collimation is shown in Table II. The energy calibration and the resolution width for elastic scattering, $W(0)$, given in Table I were obtained by measuring the scattering from a vanadium specimen.

C. Background subtraction

Measurements were made with the cassette full and empty. Some measurements were repeated with the analyzing crystal mis-set by 4° in order to measure the fast-neutron scattering. It was found for frequencies other than quaiselastic ones that the empty-cassette scattering was the same as the fast-neutron scattering when the cassette was either full or empty. This shows that (a) the neon scatters a negligible number of fast neutrons and (b) the fast-neutron scattering for most frequency transfers may be subtracted from the data by using the empty-cassette results. For quasielastic scattering a small peak occurred in the empty-cassette results because of slow neutrons scattered by the cassette. This too is eliminated from the results when the empty-cassette runs are subtracted. Scattering corrections are discussed in Sec. III. The background scattering was smoothed before subtraction. The resultant scattering is essentially the coherent neutron scattering since the incoherent cross section is small (<0.1 b). Typical constant-Q scans showing the magnitudes of the scattering from the neon relative to the background can be found in Ref. 7.

Background scattering also occurs in the monitor detector, but was only appreciable for measurements at the largest Q and ν, where the incident flux is low. Because the reactor spectrum decreases with energy the counting time is longest at the large-ν end of a scan and a greater percentage of background counts is recorded by the monitor. This effect would lead to an underestimate of the scattering from the neon at large ν if no correction were applied. The monitor background was measured with a sheet of cadmium between the monochromator and the monitor detector and all results for $S(Q, \nu)$ corrected for this background.

D. Resolution function

It is impractical to attempt to deconvolute the complete four-dimensional resolution function of the spectrometer from the scattering data. Instead, we have folded a semiempirical resolution function into the theoretical intensities for comparison with the observed intensities.[10] The most

TABLE I. Spectrometer parameters. The mosaic spreads in the monochromator and analyzer crystals are denoted $\delta\theta_m$ and $\delta\theta_a$. The energy of the scattered neutrons is E. The FWHM of the scattering from vanadium is $W(0)$.

Range of Q (Å^{-1})	Monochromator crystal (reflection)	$\delta\theta_m$	Analyzer crystal (reflection)	$\delta\theta_a$	$2\theta_a$	E/h (THz)	$W(0)$ (THz)
$0.8 \le Q \le 3.8$	Ge(111)	0.25°	PG[a] (002)	0.47°	44.88°	3.040	0.24
$3.6 \le Q \le 10.0$	Be(103)	0.20°	Be(110)	0.45°	52.25°	19.53	1.24
$10.0 \le Q \le 12.5$	Be(103)	0.20°	Be(110)	0.45°	43.00°	28.19	2.36

[a] Pyrolytic graphite.

important effects of the finite resolution of the spectrometer can be taken into account by assuming that the observed intensity $I_{\text{obs}}(\nu)$ is given in terms of the corresponding unbroadened intensity $I(\nu)$ by an expression of the form

$$I_{\text{obs}}(\nu) = \frac{\int R(\nu, \nu') I(\nu')\, d\nu'}{\int R(\nu, \nu')\, d\nu'}, \tag{2.1}$$

where the resolution function is taken to be

$$R(\nu, \nu') = \exp[-(\nu - \nu')^2/2\sigma(\nu)^2]. \tag{2.2}$$

The FWHM (full width at half-maximum) of the resolution function is given by

$$W(\nu) = (8 \ln 2)^{1/2}\sigma(\nu) = 2.35\sigma(\nu). \tag{2.3}$$

This latter quantity was determined at $\nu = 0$ from the width of the vanadium scattering (see Table I). For arbitrary frequency transfer ν, it was assumed that $W(\nu)$ was related to the monochromator setting θ_m and analyzer setting θ_a by the expression

$$W(\nu) = 2\nu_0 \cot(\theta_m)(\delta\theta_0)_{\text{eff}} + 2\nu_1 \cot(\theta_a)(\delta\theta)_{\text{eff}}. \tag{2.4}$$

The effective divergence angles of the incident and scattered beams, $(\delta\theta_0)_{\text{eff}}$ and $(\delta\theta)_{\text{eff}}$, respectively, are given essentially by a convolution of the geometric collimation with the mosaic spreads of the crystals. In general, they depend on the crystals used for each resolution range; for the particular instrumental arrangement used in this experiment they were to a good approximation equal for all three resolution ranges with values $(\delta\theta_0)_{\text{eff}} = 0.79°$ and $(\delta\theta)_{\text{eff}} = 1.12°$. The relation (2.4) is consistent with the three measured vanadium widths (Table I) to better than 4%. In Fig. 1 the quantity $W(\nu)$ is shown for the three resolution ranges. It will be seen later (Figs. 9 and 12) that the instrumental width is small compared with the observed width of the liquid scattering. Only at 2.4 and 4.5 Å^{-1} do the instrumental and observed widths become comparable.

TABLE II. Angular divergences.

	Vertical collimation	Horizontal collimation
Incident beam	1°	0.70°
Scattered beam	4°	0.66°

III. MULTIPLE SCATTERING AND NORMALIZATION

The double differential cross section for the scattering of a neutron by a macroscopic system from an initial state with wave vector $\vec{k}_0$ to a final state with wave vector $\vec{k}$ is given according to Van Hove[11] by

$$\frac{d^2\sigma}{d\Omega\, d\epsilon} = N\frac{\sigma_s}{4\pi}\frac{k}{k_0} S(Q, \omega), \tag{3.1}$$

where N denotes the number of atoms in the system, σ_s the average bound-atomic-scattering cross section, and $S(Q, \omega)$ the scattering function in which $\vec{Q}$ and ω are the momentum and energy transfers in units of $\hbar$:

$$\vec{Q} = \vec{k}_0 - \vec{k}, \quad \omega = \epsilon_0 - \epsilon. \tag{3.2}$$

Here $E = \hbar\epsilon = \hbar^2 k^2/2m_n$ is the energy of a neutron with momentum $\hbar\vec{k}$ and m_n is the neutron mass.

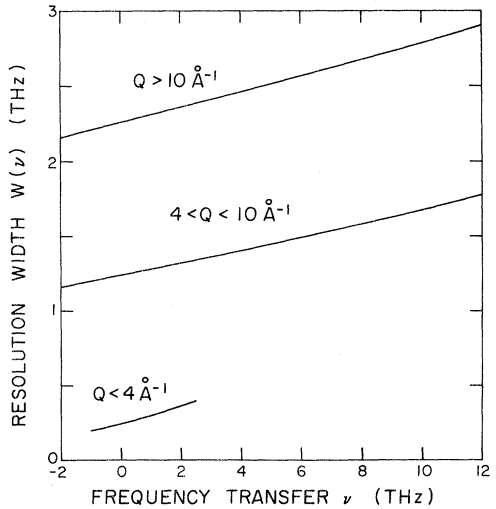

FIG. 1. Full width at half-maximum of the resolution function for each of the three resolution ranges employed in the experiments.

The expression (3.1) is valid only for a system whose linear dimensions are sufficiently small that the neutron is scattered only once by the liquid. A correction for multiple scattering is usually necessary in liquids, especially for values of Q below the position of the first diffraction maximum, where the single scattering is small and the proportion of multiple scattering is correspondingly large.

For a sample of finite size, $S(Q, \nu)$ is replaced[12] by an effective scattering function $s(\vec{k}_0, \vec{k})$, which depends on $\vec{k}_0$ and $\vec{k}$ separately and not simply on Q and ω. Also, the effective scattering function depends on the size, shape, and orientation of the sample and is not simply a bulk property of the sample, as $S(Q, \omega)$ is.

From an iterated solution of the neutron transport equation the effective scattering function can be expanded as

$$s(\vec{k}_0, \vec{k}) = \sum_{j=1}^{\infty} s_j(\vec{k}_0, \vec{k}) , \tag{3.3}$$

in which $s_j(\vec{k}_0, \vec{k})$ is the contribution from neutrons which are scattered j times. If the linear dimensions of the sample are small in comparison with the neutron mean free path the series (3.3) is rapidly convergent and only the first two terms need be retained. Explicit expressions for $s_j(\vec{k}_0, \vec{k})$ for all j in the form of multidimensional integrals can be found in Ref. 12 for a sample of arbitrary size and shape. In that reference a semianalytic method of evaluating such integrals is developed and applied to plane-slab, spherical, and cylindrical geometries.

It is found that for the present cylindrical sample the proportions of single, double, and higher-order scattering at the larger values of Q are typically 97.44%, 2.52%, and 0.04%, respectively. (Without the cadmium spacers the double scattering would have been about 6%.) The amount of multiple scattering in the present experiments is therefore comparable to that in Ref. 1, where a layered tubular geometry was employed.

The effective scattering function is given approximately by

$$s(\vec{k}_0, \vec{k}) \simeq 0.914 S(Q, \omega) + (0.024/2\pi) \int_0^{2\pi} d\phi_1 \times \int_0^{\infty} d\epsilon_1 \, S(Q_1, \omega_1) S(Q_2, \omega_2) , \tag{3.4}$$

in which the two terms represent single and double scattering. The factor 0.914 describes the reduction in the single scattering due to the attenuation of the incident and single scattered beams in the sample. This attenuation may in general contain contributions from both absorption and scattering, but for neon the absorption is negligible (<0.032 b). The attenuation from scattering reflects the fact that the double scattering occurs at the expense of the single scattering. In the second term in (3.4) the quantities $\vec{Q}_1, \omega_1$ and $\vec{Q}_2, \omega_2$ are the momentum and energy transfers in the first and second collisions:

$$\begin{aligned} \vec{Q}_1 &= \vec{k}_0 - \vec{k}_1, \quad \omega_1 = \epsilon_0 - \epsilon_1, \\ \vec{Q}_2 &= \vec{k}_1 - \vec{k}, \quad \omega_2 = \epsilon_1 - \epsilon , \end{aligned} \tag{3.5}$$

in which $\vec{k}_1$ is the momentum of the neutrons in the intermediate state. This quantity has polar coordinates (k_1, θ_1, ϕ_1) with the cylinder axis as polar axis and the integral in (3.4) is to be evaluated with $\theta_1 = \frac{1}{2}\pi$ since, in the presence of the absorbing spacers, $\vec{k}_1$ is confined to values in the neighborhood of the plane of scattering.

For a given theoretical model of $S(Q, \omega)$ one can use (3.4) to generate the corresponding effective scattering function $s(\vec{k}_0, \vec{k})$. This, in turn, can be folded with the resolution function of Sec. II D to obtain a theoretical intensity for comparison with the corresponding observed intensity $I_{\text{obs}}(\nu)$. Henceforth, unless otherwise stated, the term "scattering function" will refer theoretically to the resolution-broadened $s(\vec{k}_0, \vec{k})$ and experimentally to the normalized $I_{\text{obs}}(\nu)$.

The three normalization constants for the three resolution ranges were obtained by matching the average values of the observed and calculated scattering functions. Although the normalization is not sensitive to the model of $S(Q, \omega)$ which was employed, we mention for completeness that the memory-function model was used for the low-Q normalization and the Gram-Charlier expansion for the middle- and high-Q regions. These and other models are discussed in Sec. IV.

Figure 2 shows the calculated contributions of single and double scattering to the total scattering function of liquid neon for four representative values of Q. It is seen that the multiple-scattering correction is appreciable only when $Q \lesssim 1$ Å^{-1} or in the wings of the peaks, i.e., where the single scattering is itself small. (Note the vertical scales.) For these regions no attempt is made to draw inferences about the dynamical behavior of the liquid. Furthermore, in comparison with the single scattering, the multiple scattering is a slowly varying function of ν so that the presence of multiple scattering does not produce any qualitative distortion of the distributions, even at the smallest values of Q.

IV. THEORY

The scattering cross section of liquid neon is qualitatively different for small and large Q. For

$Q \lesssim 4$ Å^{-1} the scattering is dominated by interference effects and can be visualized as occurring as a result of the neutron creating or annihilating a collective density fluctuation in the liquid. For larger values of Q the scattering occurs essentially as a result of the collision of the neutron with a single atom in the liquid, and interference effects play only a minor though observable role.

A. Hydrodynamic limit

The classical coherent scattering function can be expressed, either with the help of linear-response theory[13] or on the basis of a continued-fraction representation,[14,15] in the form

$$S(Q,\omega) = \frac{S(Q)}{\pi} \times \frac{\omega_0(Q)^2 Q^2 \Gamma'(Q,\omega)}{[\omega^2 - \omega_0(Q)^2 + \omega Q^2 \Gamma''(Q,\omega)]^2 + [\omega Q^2 \Gamma'(Q,\omega)]^2}, \tag{4.1}$$

where $S(Q)$ is the structure factor,

$$S(Q) = \int_{-\infty}^{\infty} S(Q,\omega)\, d\omega = 1 + \rho \int e^{i\vec{Q}\cdot\vec{r}} [g(r) - 1]\, d\vec{r}, \tag{4.2}$$

in which ρ is the number density, $g(r)$ the pair correlation function, and

$$\omega_0(Q)^2 = k_B T Q^2 / m S(Q), \tag{4.3}$$

where k_B is the Boltzmann's constant, T the temperature, and m the mass of a neon atom. The quantity

$$\Gamma(Q,\omega) = \Gamma'(Q,\omega) + i\Gamma''(Q,\omega) \tag{4.4}$$

is a complex damping function or memory function whose real and imaginary parts are related by a dispersion relation which expresses the fact that $\Gamma(Q,\omega)$ is analytic in the lower half of the complex-ω plane. While (4.1) is exact for all Q, its usefulness is restricted to values of Q for which $\Gamma(Q,\omega)$ is a simpler quantity than $S(Q,\omega)$ itself.

In the hydrodynamic limit, $Q \to 0$, the scattering function,[16] and hence $\Gamma(Q,\omega)$,[14] can be obtained from the solution of the linearized Navier-Stokes and heat transport equations, and one finds that

$$\Gamma(Q,\omega) = \frac{(1 - 1/\gamma)c^2}{i\omega + aQ^2} + b, \tag{4.5}$$

in which c is the velocity of sound, $\gamma = C_p/C_v$, the specific-heat ratio, and

$$a = \lambda/m\rho C_v, \quad b = (1/m\rho)(\zeta + \tfrac{4}{3}\eta), \tag{4.6}$$

where λ is the thermal conductivity, η the shear viscosity, and ζ the bulk viscosity. It follows with the help of the thermodynamic and transport properties of liquid neon at 26.9 °K listed in Table III that $a = 1.05 \times 10^{-3}$ cm^{2}sec^{-1} and $b = 2.11 \times 10^{-3}$ cm^{2}sec^{-1}. The first term in the expression (4.5) for $\Gamma(Q,\omega)$ gives the contribution to the damping due to heat conduction and the second term the contribution from viscosity.

B. Memory-function model

For the Q values employed in slow-neutron inelastic-scattering experiments Q^{-1} is comparable to the interatomic spacing in the liquid, so that the hydrodynamic limit is not applicable. For such values of Q it may be appropriate to adopt a model of the form[13,15,22]

$$\Gamma(Q,\omega) = \frac{A(Q)}{i\omega + \alpha(Q)} + \frac{B(Q)}{i\omega + \beta(Q)}, \tag{4.7}$$

in which the coefficients are chosen such that[15] (i) $\Gamma(Q,\omega)$ is analytic in the lower half of the complex-ω plane, (ii) $\Gamma(Q,\omega)$ reduces to the hydrodynamic limit (4.5) as $Q \to 0$, (iii) the zero-, second-, and fourth-moment relations are satisfied identically for all Q, (iv) $S(Q,\omega)$ has approximately the correct asymptotic form as $Q \to \infty$.

While these conditions do not determine the coefficients in (4.7) uniquely, it is not unreasonable to expect that a suitable model which satisfies them might be at least qualitatively correct for the Q values of interest. The explicit expressions for the coefficients which we have used are given in Ref. 15 and need not be reproduced here. We simply point out that the model contains no adjust-

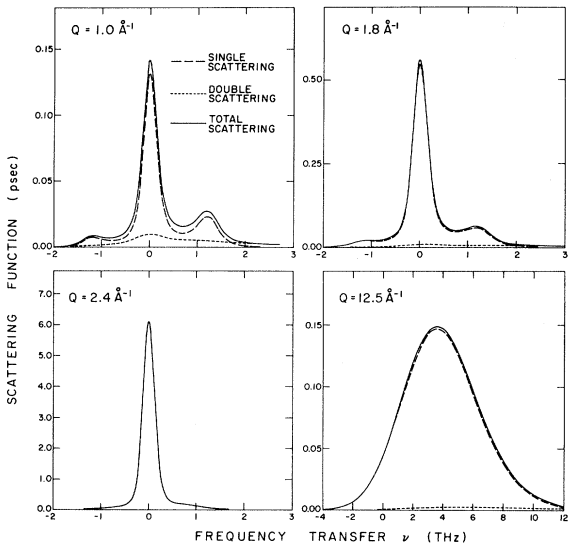

FIG. 2. Calculated contributions of single and double scattering to the total scattering in liquid neon at 26.9 °K for four representative values of Q. The calculations at $Q = 12.5$ Å^{-1} were made on the basis of the Gram-Charlier expansion and the remaining three on the basis of the memory-function model.

TABLE III. Thermodynamic and transport properties of orthobaric liquid neon at $T = 26.9\,^{\circ}\mathrm{K}$.

Quantity	Value	Ref.
Lennard-Jones parameters	$\epsilon/k_B = 35.6\,^{\circ}\mathrm{K}$	6
	$\sigma = 2.75$ Å	6
Number density	$\rho = 3.61\times 10^{22}$ atoms/cm^3	17
Reduced number density	$\rho^* = \rho\sigma^3 = 0.751$	
Reduced temperature	$T^* = k_B T/\epsilon = 0.756$	
Specific heat at constant volume	$C_v = 17.9J$ mol^{-1}deg^{-1}	17
Specific heat at constant pressure	$C_p = 37.5J$ mol^{-1}deg^{-1}	17
Specific-heat ratio	$\gamma = C_p/C_v = 2.09$	
Velocity of sound	$c = 5.91\times 10^4$ cm sec^{-1}	18
Adiabatic compressibility	$K_S = 1/m\rho c^2 = 2.40\times 10^{-4}$ atm^{-1}	
Isothermal compressibility	$K_T = \gamma K_S = 5.02\times 10^{-4}$ atm^{-1}	
Compressibility limit of structure factor	$S(0) = \rho k_B T K_T = 0.0664$	
Thermal conductivity	$\lambda = 1.13\times 10^{-3}$ Wcm^{-1}deg^{-1}	19
Shear viscosity	$\eta = 1.26$ mP	20
Bulk voscosity	$\zeta = 0.87$ mP	21

able parameters as far as the analysis of the neutron data is concerned; the parameters are determined uniquely by the thermodynamic and transport coefficients in Table III, by molecular-dynamics data,[23,24] and by the observed x-ray structure factor.[25] In particular, the coefficients involve the integral

$$\int (1-\cos Qx)\frac{\partial^2\phi(r)}{\partial x^2}g(r)\,d\vec{r}, \tag{4.8}$$

in which $\phi(r)$ is the pair potential. This integral was evaluated numerically on the basis of the Lennard-Jones potential.[6] The pair correlation function was that obtained by Verlet[24] in a molecular-dynamics calculation for a Lennard-Jones liquid with $T^* = 0.827$ and $\rho^* = 0.750$. A check on the accuracy of the numerical integration is obtained by noting that as $Q \to \infty$ the integral (4.8) is proportional to $\langle \Delta\phi \rangle$ and hence[26] to the mean square force on an atom. The latter quantity can also be obtained directly from the molecular-dynamics results,[23] and the two values are found to differ by only 3%. When Verlet's pair correlation function was used in (4.2) to evaluate the structure factor, problems were encountered at small Q arising from the truncation of $g(r)$ at large r. We therefore chose instead to use the observed x-ray structure factor[25] for liquid neon at 26.6 °K in the calculation of $S(Q, \omega)$.

The memory-function model (4.7) is constructed such that it reduces to the hydrodynamic limit as $Q \to 0$. [The exponential memory-function model,[2] which corresponds to $B(Q) = 0$ with $\alpha(Q)$ independent of Q, does not satisfy the hydrodynamic limit and is not considered in this paper.] The scattering function $S(Q, \omega)$ for (4.7) is found to agree with the hydrodynamic limit to better than 5% for values of Q up to 0.01 Å^{-1}, while qualitative agreement persists up to about 1 Å^{-1}. For example, it is seen in Fig. 3 that at $Q = 0.1$ Å^{-1} the memory-function model still has the triplet structure characteristic of the hydrodynamic limit. The central line at $\omega = 0$ corresponds to the decay of a density fluctuation by heat diffusion and the Brillouin doublet at $\omega = \pm cQ$ corresponds to the propagation of the density fluctuation as a sound wave which subsequently decays by viscosity and heat conduction. The persistence of the Brillouin structure in the memory-function model for liquid neon up to such large Q values was unexpected in view of our previous experience with liquid argon,[15] where the sound-wave peaks disappear at about $Q = 0.05$ Å^{-1}. However, as the present paper was being prepared for publication we learned that such distinct sound-wave peaks have been observed by neutron inelastic scattering in liquid neon[27] for $0.06 \leq Q$

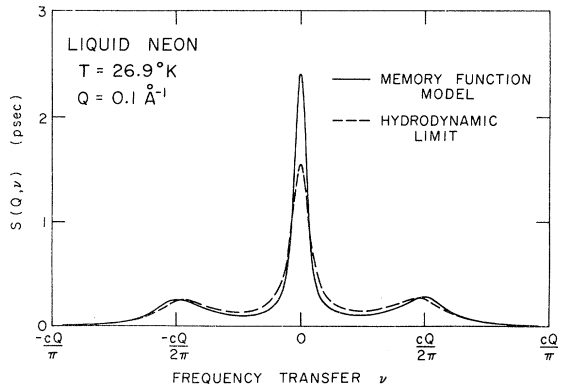

FIG. 3. Comparison of the memory-function model for $S(Q, \omega)$ with the corresponding hydrodynamic limit at $Q = 0.1$ Å^{-1}.

$\lesssim 0.14$ Å^{-1} and also in liquid rubidium[28] for $Q<1$ Å^{-1}.

The expression (4.1) for $S(Q,\omega)$ is classical, so that it is an even function of ω and hence neglects effects of translational recoil and detailed balance. These are small effects in liquid neon when $Q\lesssim 4$ Å^{-1} and can be taken satisfactorily into account by including in (4.1) the usual factor[29]

$$\exp\left(\frac{\hbar\omega}{2k_BT}-\frac{\hbar^2Q^2}{8mk_BT}\right). \tag{4.9}$$

While quantum effects in the liquid itself are not taken explicitly into account in the memory-function model, they are to some extent accounted for by using experimental values for the thermodynamic and transport properties.

C. Impulse approximation

In the limit $Q\to\infty$ the impulse approximation (IA) provides an asymptotically exact description of the scattering. In the IA the scattering atom recoils as if it were free and the scattering function is just the Doppler profile characteristic of the velocity distribution $p(\vec{v})$ of the atoms in the initial state[30,31]:

$$S_{IA}(Q,\omega)=\int p(\vec{v})\delta(\omega-\omega_r-\vec{Q}\cdot\vec{v})\,d\vec{v}, \tag{4.10}$$

in which $\omega_r=\hbar Q^2/2m$ is the recoil energy and the δ function expresses conservation of energy and momentum in the collision of a neutron with a neon atom having initial velocity $\vec{v}$.

For a classical system in thermodynamic equilibrium at temperature T, the velocity distribution is Maxwellian,

$$p(\vec{v})=(4\pi u^2)^{-3/2}e^{-(v/2u)^2}, \tag{4.11}$$

where $u=(k_BT/2m)^{1/2}$, so that

$$S_{IA}(Q,\omega)=\frac{1}{2(\pi)^{1/2}Qu}\exp\left[-\left(\frac{\omega-\omega_r}{2Qu}\right)^2\right]. \tag{4.12}$$

There is a tendency to confuse the IA with free-atom scattering because $p(\vec{v})$, and hence $S_{IA}(Q,\omega)$, are the same classically for a liquid as for an ideal gas. The distinction becomes important for liquid neon[31] and even more so for liquid helium,[30] in which quantum effects produce an appreciably non-Maxwellian velocity distribution. Since quantum effects are relatively small in liquid neon one can employ an expansion in powers of $\hbar$. In this case one finds[32] that (4.11), and hence (4.12), remain formally unchanged to order $\hbar^4$, but the quantity u becomes

$$u=(k_BT/2m)^{1/2}(1+q), \tag{4.13}$$

where

$$q=\hbar^2\langle\Delta V\rangle_{cl}/72m(k_BT)^2. \tag{4.14}$$

Here V is the total potential energy, Δ the Laplacian with respect to the position of one atom in the system, and $\langle\cdots\rangle_{cl}$ denotes the average over a classical equilibrium canonical ensemble at temperature T. The quantity $\langle\Delta V\rangle_{cl}$ can be obtained as discussed in Sec. IV B, and one finds that $q=0.137$ at 26.9 °K. (This value of q differs from our earlier less accurate estimate in Ref. 7.) The next quantum correction to u is[31] approximately $-(17/10)q^2$, so that

$$u\simeq(k_BT/2m)^{1/2}(1+q-\tfrac{17}{10}q^2)=(k_BT/2m)^{1/2}(1.105). \tag{4.15}$$

Thus quantum effects in liquid neon increase the value of u, and hence the width of the scattering function, by about 10%.

D. Gram-Charlier expansion

For a finite value of the wave-vector transfer Q the scattering atom is inhibited by interatomic forces from recoiling freely. If these forces were so strong that the atom were held at a fixed point in space, the scattering would be perfectly elastic and $S(Q,\omega)$ would reduce to $\delta(\omega)$. In fact, the final-state interactions are not strong enough to inhibit the recoil completely, although they do produce a narrowing of the scattering function. The narrowing can conveniently be represented by means of an expansion of the scattering function in terms of Hermite polynomials,[30,31,33-35]

$$S(Q,\omega)=\frac{1}{2(\pi)^{1/2}Qu}\exp\left[-\left(\frac{\omega-\omega_r}{2Qu}\right)^2\right]\times\sum_{n=0}^{\infty}\epsilon_n(Q)H_n\left(\frac{\omega-\omega_r}{2Qu}\right). \tag{4.16}$$

Expressions for $\epsilon_n(Q)$ for $n=0$, 1, 2, 3, 4 are given in Ref. 33 and will not be reproduced here. They involve the same integrals as occur in the memory-function model (Sec. IV B). For liquid neon, in which quantum effects are smalll, the correction to the impulse approximation due to final-state interactions is adequately represented by truncating the Gram-Charlier expansion (4.16) beyond the $n=4$ term.[31]

E. Kerr-Singwi model

Finally, the neon data will also be compared with recent calculations of Kerr and Singwi[36] based on a generalized mean-field approximation involving the polarization potential and the screened response function. The latter quantity is closely related to the memory function of Sec. IV A. While our memory-function model has been constructed to give the correct hydrodynamic limit, and hence

is essentially a small-Q theory, the Kerr-Singwi model for the screened response function is constructed to give correctly the impulse approximation at large Q. Although the Kerr-Singwi model does not satisfy the hydrodynamic limit, it will be found to give quite reasonable results for values of Q down to the region of the first diffraction maximum.

The published theory of Kerr and Singwi[36] was evaluated for $1.6 \leq Q \leq 12.5$ Å^{-1} with the aid of the pair correlation function $g(r)$ of Verlet,[24] which was Fourier transformed to give $S(Q)$. At $Q = 1.6$ Å^{-1} the resultant $S(Q)$ is 1.48 times smaller than the observed x-ray structure factor of Stirpe and Tompson.[25] Kerr has informed us that this is probably a result of termination error in the Fourier transformation and he has sent us new calculations using the x-ray $S(Q)$. For $Q \leq 2.0$ Å^{-1} these are the calculations that will be discussed later in reference to Figs. 7–9. The quantum correction used by Kerr and Singwi, since it involved only the linear term in q with the value $q = 0.142$, is larger than the more accurate correction we have evaluated in Sec. IV C. It will be seen to lead to too large a width of the peak in $S(Q, \omega)$ at large Q.

V. RESULTS

Neutron-inelastic-scattering results were obtained from $Q = 0.8$ to 3.8 Å^{-1} in steps of 0.2 Å^{-1} and from 4.5 to 12.5 Å^{-1} in steps of 0.5 Å^{-1}. They are compared in this section with the theory of Sec. IV. The present experiment leads to a quite different picture of the dynamics of liquid neon than was suggested by Chen *et al.*[37] in analyzing their time-of-flight results; the reasons for this are discussed. All experimental data have been normalized to an absolute scale by the method described in Sec. III. Errors on the points where indicated are the combined errors in counting the signal and the background. With the exception of the data for $S(Q)$, where the multiple scattering has been subtracted, all comparisons are made for the line shapes actually observed. Thus, as discussed in Secs. II and III, the observed scattering functions and corresponding widths and peak positions have been corrected only for background scattering, but not for multiple-scattering and resolution effects. Instead, multiple-scattering and resolution corrections have been applied to the theoretical scattering functions before comparing with experiment. An exception is the Kerr-Singwi model, which was corrected only for resolution effects. The results sent to us by Kerr were in a form not compatible with our multiple-scattering program. The other models show, however, that multiple scattering was small except when $Q \lesssim 1$ Å^{-1} (see Fig. 2).

It will be noted that a different procedure was followed in preliminary reports of this work.[7,36] There the observed widths and peak positions were corrected approximately for both background and instrumental resolution, but not multiple scattering, and the corrected data were then compared directly with the corresponding theoretical predictions. The procedure followed in the present paper is more accurate.

A. Structure factor

The structure factor $S(Q)$ was obtained by integrating the data for each constant-Q scan over all frequencies. Measurements were made over a frequency range large enough that no extrapolation of the wings was necessary to obtain $S(Q)$.

The results for $S(Q)$ are shown in Fig. 4 and are in satisfactory agreement with the x-ray structure factor of Stirpe and Tompson.[25] The x-ray data are shown since they cover a wider range of Q values, and are probably more accurate, than the earlier neutron-diffraction data of Henshaw.[38] The agreement between the present results and the x-ray results at the narrow first diffraction maximum shows that the finite wave-vector resolution does not materially influence the results. At other wave vectors, where $\partial^2 S(Q, \omega)/\partial^2 Q$ is much smaller, the error from this cause will be negligible. At low wave vectors, $S(Q)$ tends to the compressibility limit (see Table III), which is indicated by the cross in Fig. 4. The compressibility limit is consistent with both the neutron and x-ray data. No comparison can be made with the work of

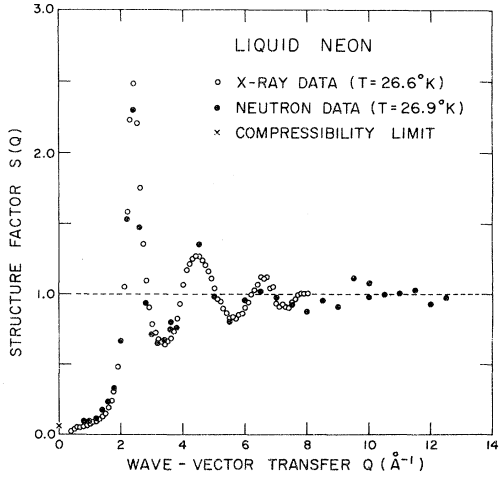

FIG. 4. Comparison of the structure factor of liquid neon determined in the present neutron-scattering experiments with that obtained by x-ray diffraction (Ref. 25).

de Graaf and Mozer,[39] who observed oscillations of ~1% of $S(Q)$ persisting out to 12 Å^{-1}, because they studied neon at different pressures and temperatures (>21.4 atm and 35.05 °K).

B. General behavior of $S(Q,\nu)$

A global view of the observed scattering function of liquid neon is given by the contour plots in the (Q, ν) plane shown in Figs. 5 and 6. In constant-Q scans the scattering function falls monotonically from its peak value. At the wave vectors studied, therefore, the density fluctuations in the liquid are not well defined in frequency. In constant-ν scans the scattering function can exhibit as many as three peaks at small frequency. Fluctuations of the same frequency do, therefore, exhibit a spatial coherence. The spatial coherence is similar to that of the pair distribution function and merely indicates that even moving atoms in a liquid are arranged with considerable local order.

The neutron scattering is displaced to positive frequencies (neutron energy loss) by an amount that increases with increasing Q. At large Q the peak lies close to the single-particle recoil frequency, $\nu_r = \hbar Q^2/4\pi m$, which is indicated by the thick line in the upper part of Fig. 5. At small Q the asymmetry is apparent, even near the peak of the structure factor, and reflects the nonclassical nature of liquid neon. For all Q the scattering function should obey the detailed-balance condition

$$S(Q, \nu) = e^{\beta\nu} S(Q, -\nu), \tag{5.1}$$

where $\beta = h/k_B T$. The extent to which the data satisfy this condition is shown by the symmetrized scattering function

$$\hat{S}(Q, \nu) = e^{-\beta\nu/2} S(Q, \nu), \tag{5.2}$$

plotted in Fig. 6. It is seen that this quantity is essentially an even function of ν, as it should be according to (5.1). Thus, for example, the peak occurs close to zero frequency (-0.17 ± 0.20 THz) even at 10 Å^{-1}, where the recoil frequency is as large as 2.5 THz. In view of the large line-shape change produced by the exponential factor in (5.2) and the large value of analyzer energy (19.53 THz), it is concluded that the results are consistent with detailed balance.

C. Collective regime

For wave-vector transfers less than 4 Å^{-1} the scattering from liquid neon can best be regarded as arising from the collective motion of many atoms. The line shapes, some of which are shown in Fig. 7, are seen to consist of a relatively sharp central peak with wings which are most pronounced

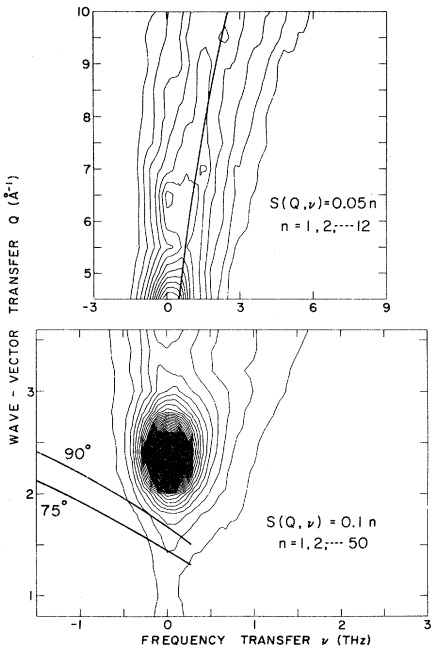

FIG. 5. Contour plot of the observed scattering function of liquid neon at 26.9 °K. The irregularities in the contours are a reflection of the statistical fluctuations in the observed counting rates. The smooth curve in the upper figure is the recoil frequency $\nu_r = \hbar Q^2/4\pi m$. The smooth curves in the lower figure show the (Q, ν) values sampled in the time-of-flight experiments of Ref. 37 for angles of scattering of 75° and 90°.

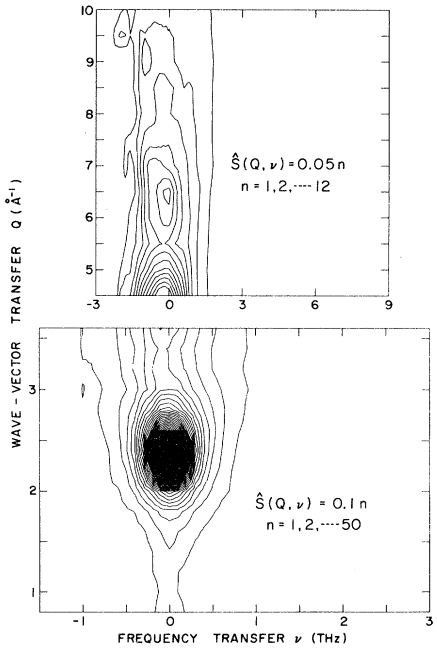

FIG. 6. Contour plot of the observed symmetrized scattering function of liquid neon at 26.9 °K.

at positive-frequency transfers. The wing is scarcely visible at the peak of the structure factor, $Q = 2.4$ Å^{-1}, but this is because the central component there is very intense (note the vertical scale changes). Indeed the scattering, e.g., at 1 THz, is of comparable intensity for all wave vectors in the collective regime; it increases gradually with increasing Q. For $Q \leq 1.6$ Å^{-1} there is evidence for a shoulder near ~1.2 THz, but the statistical accuracy is not sufficient to regard this as firm evidence for a peak.

Beyond the peak in the structure factor the distinction between central component and wing becomes less clear. The line shapes are smooth and featureless, with the exception of the scans at 3.2 and 3.4 Å^{-1}. The latter is displayed in Fig. 7 and suggests that a shoulder exists in the vicinity of 1 THz.

It is concluded on the basis of the experimental results that in the collective regime between 0.8 and 3.8 Å^{-1} there is no evidence for any well-defined inelastic peak in the spectrum of density fluctuations. On the other hand, the existence of inelastic wings below 1.6 Å^{-1} does reflect collective motion in the liquid, since such wings would be absent if each atom moved independently according to laws of simple diffusion.

The theoretical results for the line shapes are compared with experiment in Fig. 7. The memory-function theory of Sec. IV B overemphasizes the magnitude of the inelastic scattering within the wing, and a peak at finite frequency is predicted. The central peak is too narrow. In contrast, the Kerr-Singwi model[36] has too wide a central peak and the inelastic structure in the wing is absent. It is possible that the shoulder seen in the experiment at 1.2 THz corresponds to the peak predicted by the memory-function theory, but is partially washed out by the stronger damping which is actually present. Thus the behavior of liquid neon is intermediate between the quasielastic overdamped response of liquid argon[1,2] and the well-defined-phonon type of response in liquid helium.[3] In liquid hydrogen[4] and liquid rubidium,[28] where a long inelastic wing terminating in a peak is observed, the scattering appears to be intermediate between neon and helium as far as damping of the one-phonon response is concerned.

The peak height of the scattering function is shown in Fig. 8. Both theories give peak heights that are larger than experiment at the first diffraction maximum but are in satisfactory agreement elsewhere. The effects of finite wave-vector resolution are important only near the first diffraction maximum, and will tend to make the experimental results low (~10%) in this region.

The FWHM of the scattering function (Fig. 9) shows that large differences exist between the theories and also between either theory and experiment. Only near 2.4 Å^{-1} are both theories in reasonable agreement with experiment. For $Q > 2.4$ Å^{-1} the Kerr-Singwi theory predicts the observed width remarkably well, but for $Q < 2.0$ Å^{-1} neither theory is in agreement with experiment. The experimental results lie between the two theoretical lines but tend towards the memory-function results at the lowest wave-vector transfer, $Q = 0.8$ Å^{-1}. The agreement here is expected because

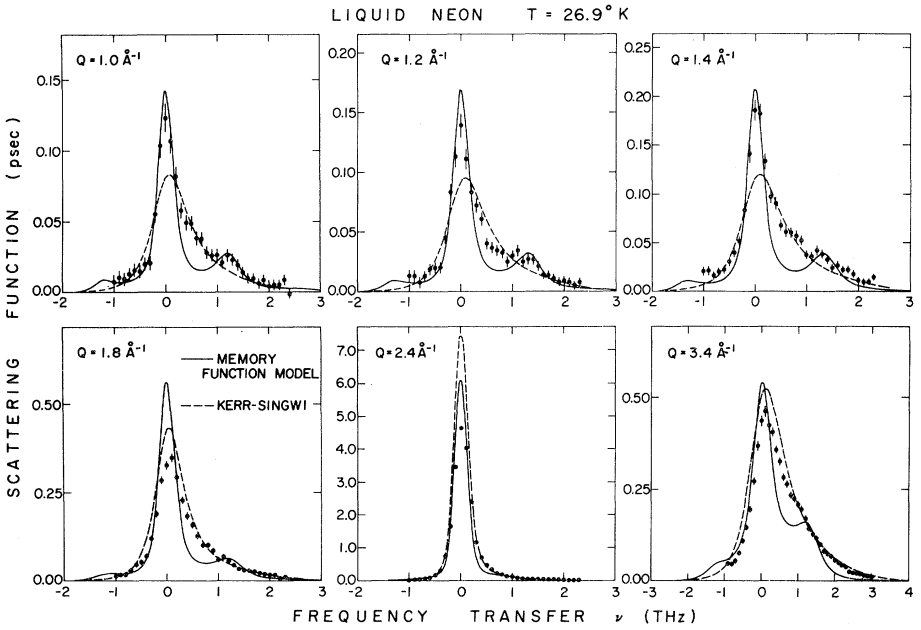

FIG. 7. Comparison of the observed scattering function of liquid neon with the results of the memory-function and Kerr-Singwi models for selected values of Q in the collective regime.

the memory-function model is consistent with the hydrodynamic limit. At other values of Q, however, the memory-function widths are too small, whereas the Kerr-Singwi widths are too large. For liquid argon Sköld *et al.*[1] found similar behavior: The screened-response type of theory gives widths that are too large.

D. Single-particle regime

As the wave-vector transfer increases the center of the scattering shifts to positive values of ν while its width increases, becoming proportional to Q at large Q in accordance with the impulse approximation (4.12). This general behavior is visible in the line shapes of Fig. 10. (Additional line shapes can be found in Ref. 7.)

Oscillations are observed in both the frequency and width of the single-particle peak out to at least 8 $Å^{-1}$. The amplitude of the oscillations gradually decreases with Q but is generally larger than the amplitude of the oscillation in $S(Q)$. The oscillations show up clearly in four characteristic properties of the line shape: the peak height (Fig. 11), the FWHM (Fig. 12), the mean frequency (Fig. 13) defined as the frequency halfway between the half-height points, and the frequency of the maximum (Fig. 14). The breaks in the curves at 10 $Å^{-1}$, when they occur, correspond to the transition between different ranges of spectrometer resolution.

The data of Figs. 11–14 shows that the periodicity of the oscillations is somewhat larger than 2 $Å^{-1}$ and thus comparable with the wave vector of the first diffraction maximum. The amount by which the frequency of the maximum is less than the recoil frequency ν_r tends to a constant[30] at large Q. The observed data in Fig. 14 are consistent with this result, as are also the predictions of the Kerr-Singwi and Gram-Charlier models.

In general, both the Gram-Charlier and Kerr-Singwi theories give a fair description of the experimental results in the single-particle regime particularly at smaller wave vectors. Below 7 $Å^{-1}$ both theories agree with experiment, showing that a maximum in the peak height is accompanied by a minimum in the width and by a minimum in either definition of frequency (Figs. 11–14). At wave vectors larger than 7 $Å^{-1}$ the oscillations continue with little change in the Kerr-Singwi theory, but in the Gram-Charlier theory they damp out rather suddenly. This surprising feature of the Gram-Charlier theory is in accord with the experimental results.

At the largest wave vectors, 10–12 $Å^{-1}$, the two theories differ by an almost constant amount in their predictions. The Kerr-Singwi theory has too small a peak height (Fig. 11) and too large a width (Fig. 12), a discrepancy that is consistent with their use of too large a quantum correction (see Sec. IV E).

Of the two definitions of the frequency of the peak, the frequency of the maximum (Fig. 14) is more sensitive to the oscillations and to the differences between the two theories. The displacement of the frequency of the Kerr-Singwi theory below the observed frequency is most marked at 7 and 8.5 $Å^{-1}$ and can be seen directly in the line shapes of Fig. 10.

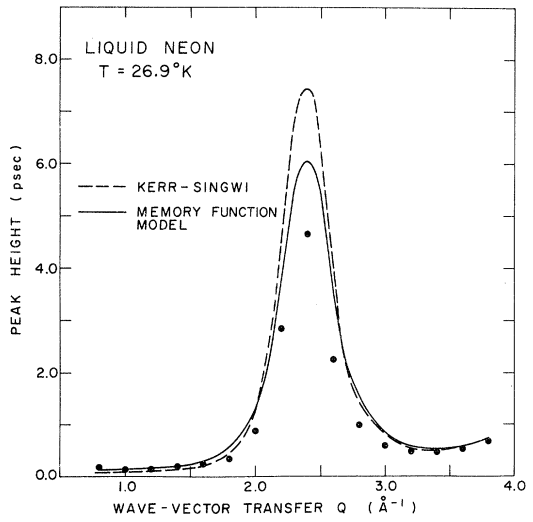

FIG. 8. Comparison of the peak height of the observed scattering function of liquid neon with the results of the memory-function and Kerr-Singwi models for Q values in the collective regime.

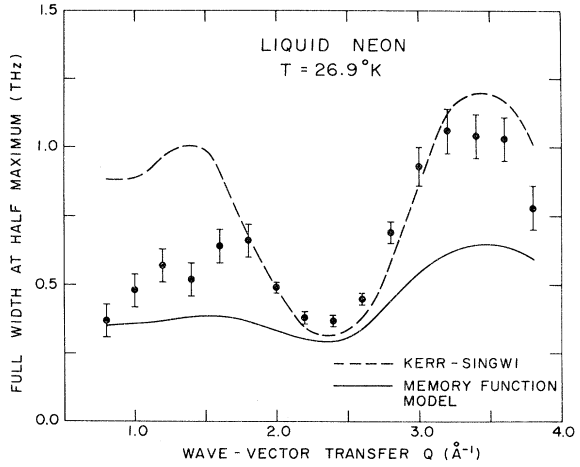

FIG. 9. Comparison of the full width at half-maximum of the observed scattering function of liquid neon with the results of the memory-function and Kerr-Singwi models for Q values in the collective regime.

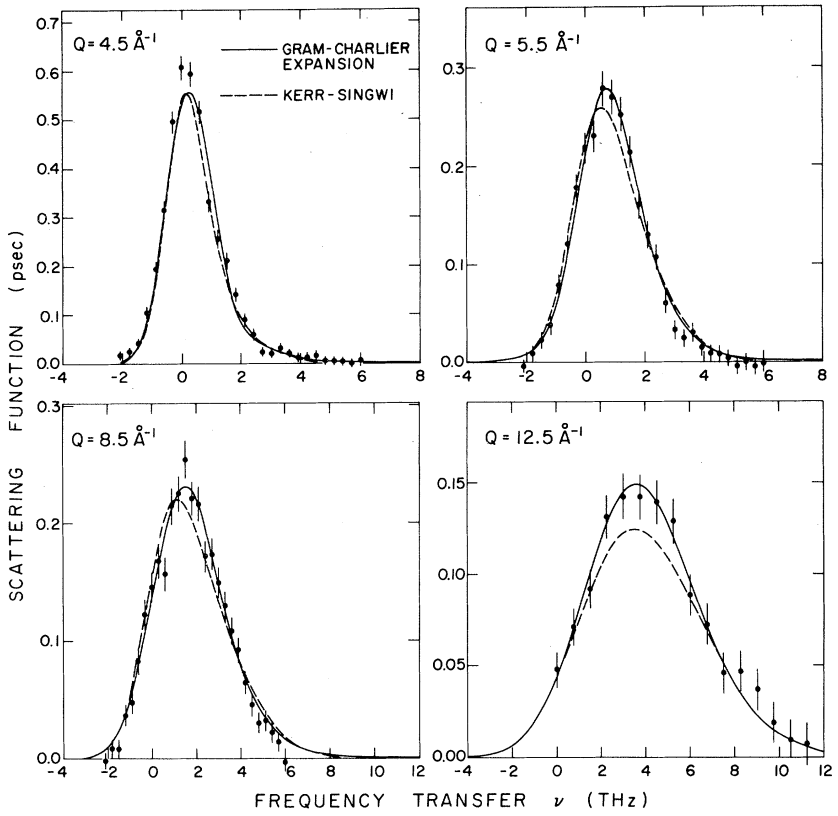

FIG. 10. Comparison of the observed scattering function of liquid neon at $T = 26.9\,^{\circ}\mathrm{K}$ with the results of the Gram-Charlier expansion and Kerr-Singwi model for selected values of Q in the single-particle regime.

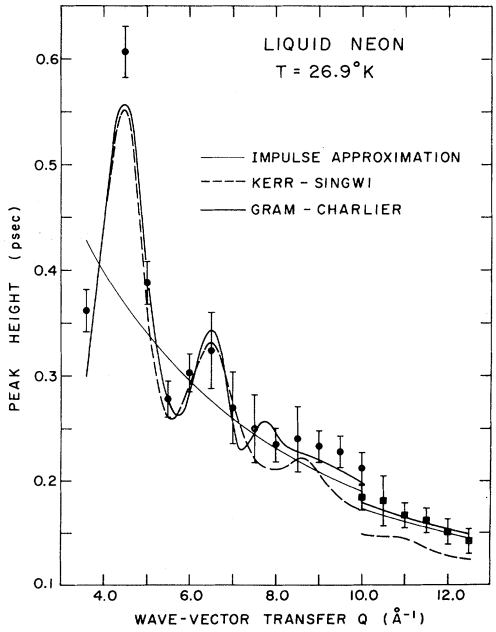

FIG. 11. Comparison of the peak height of the observed scattering function of liquid neon with the results of the impulse approximation, the Kerr-Singwi model, and the Gram-Charlier expansion for Q values in the single-particle regime.

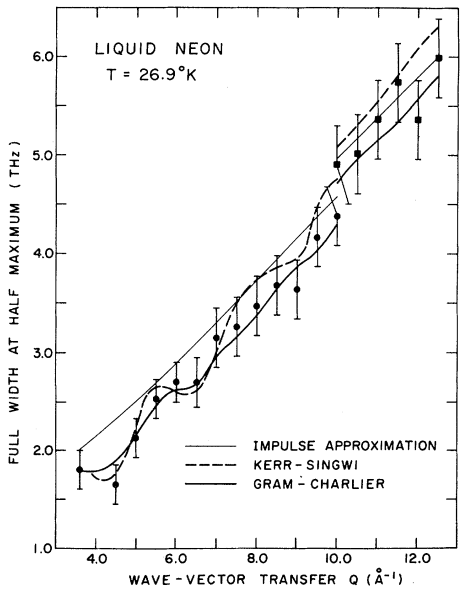

FIG. 12. Comparison of the full width at half-maximum of the observed scattering function of liquid neon with the results of the impulse approximation, the Kerr-Singwi model, and the Gram-Charlier expansion for Q values in the single-particle regime.

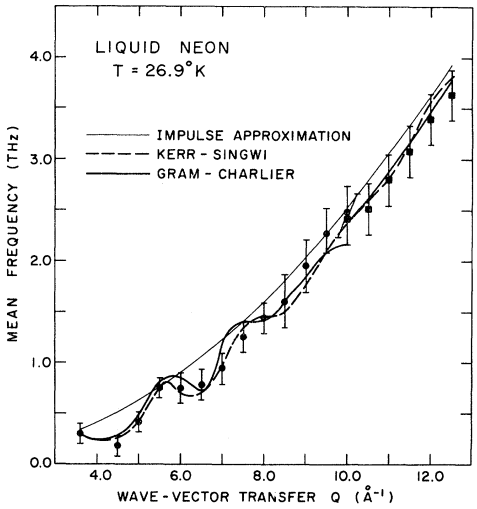

FIG. 13. Comparison of the mean frequency of the observed scattering function of liquid neon with the results of the impulse approximation, the Kerr-Singwi model, and the Gram-Charlier expansion for Q values in the single-particle regime.

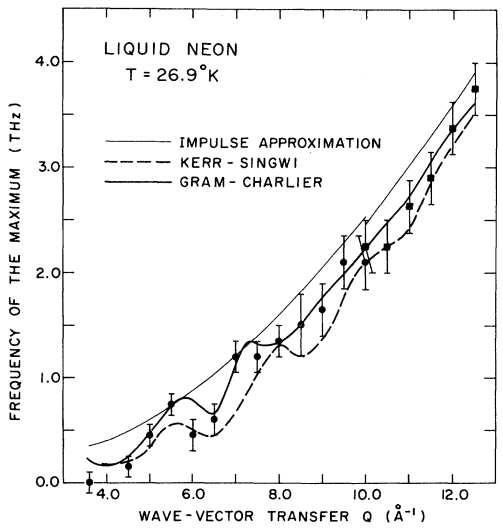

FIG. 14. Comparison of the frequency of the maximum of the observed scattering function of liquid neon with the results of the impulse approximation, the Kerr-Singwi model, and the Gram-Charlier expansion for Q values in the single-particle regime.

An objective comparison between theory and experiment is provided by the results of the χ test of Table IV. The observed value of a line-shape parameter S_i for each data point i is compared with the corresponding theoretical value and the experimental standard deviation σ_i on each of the N data points. The expression

$$\chi \equiv \left(\sum_{i=1}^{N} \frac{[S_i(\text{theor}) - S_i(\text{expt})]^2}{\sigma_i^2} \Big/ (N-1) \right)^{1/2} \quad (5.3)$$

is the rms deviation of the theory from experiment as a fraction of the error on each data point, and the summation over i includes every wave vector Q_i in scans extending from 4.5 to 12.5 Å^{-1}. Table IV shows that the normalized rms error of the Gram-Charlier model is half that of the Kerr-Singwi model when S_i is the peak height or frequency of the maximum. The other two parameters of the line shape are less sensitive; the Kerr-Singwi model is better for the mean frequency but the Gram-Charlier model is better for the FWHM. Since χ for the Gram-Charlier model is found to be consistently less than unity, it is concluded that the errors on the experimental data are in fact smaller than has been assumed. Most of the error in the Kerr-Singwi theory comes from the results for large wave vectors.

E. Comparison with time-of-flight data

Earlier neutron-scattering work on liquid neon was carried out by Chen *et al.*,[37] who use a time-of-flight technique. Their data were taken in a slab geometry where multiple scattering is large.[12] Their scattered-neutron spectrum showed two broad peaks, of which one was close to the elastic position and the other was at a significant neutron energy gain. They suggested that the peaks might correspond to damped cooperative modes, and published a figure showing the values of ν and Q at which the peaks occurred.

Paradoxically, the results of Chen *et al.*,[37] when correctly interpreted, agree with the present results, which show that there is no well-defined inelastic peak in $S(Q, \nu)$ at constant Q. The reason

TABLE IV. χ test of the Gram-Charlier expansion and Kerr-Singwi model for the range $4.5 \leq Q \leq 12.5$ Å^{-1}.

Quantity	Gram-Charlier expansion	Kerr-Singwi model
Peak height	0.77	1.67
Full width at half-maximum	0.54	0.80
Mean frequency	0.72	0.47
Frequency of maximum	0.70	1.41

for the apparently different raw spectra is that a time-of-flight experiment measures $d^2\sigma/d\Omega\, d\lambda$, where λ is the scattered-neutron wavelength which is proportional to the time of flight. Since for scattering angle ϕ and incident wavelength λ_0

$$Q=\frac{2\pi}{\lambda_0}\left[1+\left(\frac{\lambda_0}{\lambda}\right)^2-\left(\frac{2\lambda_0}{\lambda}\right)\cos\phi\right]^{1/2} \tag{5.4}$$

and

$$\nu=\frac{h}{2m}\left\{\frac{1}{\lambda_0^2}-\frac{1}{\lambda^2}\right\}, \tag{5.5}$$

it follows, when account is taken of the k/k_0 factor in the cross section (3.1), that

$$\frac{d^2\sigma}{d\Omega\, d\lambda}\sim\frac{S(Q,\nu)}{\lambda^4}. \tag{5.6}$$

The λ^4 factor varies rapidly, particularly when long-wavelength neutrons are up-scattered by the liquid, as in the experiment of Chen *et al.*,[37] who used 5.3-Å neutrons. The result is that a broad quasielastic peak in $S(Q,\nu)$ becomes a peak displaced to finite frequency in a time-of-flight experiment. A similar conclusion was reached by Cowley.[40] There is, in addition, the problem that Q varies throughout the time-of-flight (TOF) spectrum. In the present experiment $S(Q,\nu)$ is measured directly, since a constant-Q measurement was made with variable ϵ_0, as is possible with a triple-axis crystal spectrometer (TACS).[41]

The TOF data of Chen *et al.*[37] have been corrected to $S(Q,\nu)$ via (5.6) and are compared in Fig. 15 with the present TACS results. The TACS results were interpolated to find the scattering on the two (Q,ν) contours (see Fig. 5) that correspond to the TOF spectra with scattering angles of 75° and 90°. The present TACS results are on an absolute scale and the TOF results have been multiplied by a single normalization factor to bring them into approximate coincidence with the present results at neutron energy gain.

The comparison of Fig. 15 shows that the results of Chen *et al.*[37] agree with the present TACS results, particularly for neutron energy gain where the TOF experiment is accurate. (Note the large error bars at large λ.) The prominent peak at $\lambda=4$ Å in the original uncorrected time-of-flight data for $\phi=75°$ (Fig. 1 of Ref. 37) is absent from $S(Q,\nu)$. The original TOF data for $\phi=90°$ showed one peak at $\nu=-0.28$ THz but, when corrected to $S(Q,\nu)$, the peak position returns, as expected, to $\nu=0$.

Chen *et al.*'s[37] work thus supports our conclusion that there are no well-defined excitations in liquid neon for $Q>0.8$ Å^{-1}. It also illustrates that incorrect conclusions can be drawn from plots of the frequencies of peaks in uncorrected time-of-flight spectra.

VI. DISCUSSION

The dynamics of liquid neon have been studied with neutron inelastic scattering for $0.8\leq Q\leq 12.5$ Å^{-1}. In the collective regime the scattering at constant Q consists of a central diffusive peak and a monotonically decreasing inelastic wing. There are no well-defined inelastic peaks, although weak shoulders exist.

Inelastic peaks have been observed in neon at smaller wave vectors by Bell *et al.*[27] However, the results for $0.06\leq Q\leq 0.14$ Å^{-1} were at densities and temperatures ($\rho=0.48$ gm/cm^3, 70 °K) quite different from those studied in the present experiment ($\rho=1.21$ gm/cm^3, 26.9 °K). By this means Bell *et al.* reduced the sound velocity and made the low-Q region more accessible to neutrons. A shoulder was observed on the side of the quasielastic peak which became a peak at the lowest Q for neutron energy gain, while weaker scattering was observed at neutron energy loss. Since the experiment was with variable scattered neutron energy the measured quantity is[41] proportional to $S(Q,\nu)\cos\theta_a/\lambda^4$. The observed scan is therefore distorted in a similar way to a time-of-flight scan as discussed in Sec. V E. Although

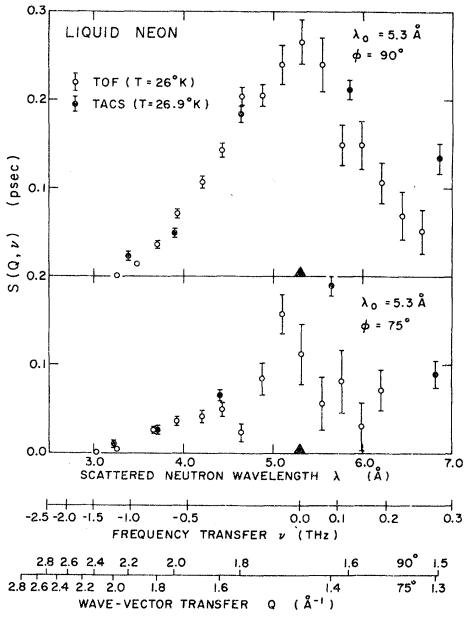

FIG. 15. Comparison of $S(Q,\nu)$ for liquid neon as determined by the time-of-flight (TOF) measurements of Ref. 37 and by the triple-axis crystal-spectrometer (TACS) data from the present experiments. The paths in (Q,ν) space for which the data are given are shown in Fig. 5.

they do not show the result, Bell *et al.*[27] state that when they correct their data a peak appears also on the neutron-energy-loss side, as we would expect from detailed balance. The observation of Brillouin peaks is consistent with the present memory-function theory, which predicts well-defined peaks at these wave vectors (see Fig. 3). A detailed comparison with the results of Bell *et al.* is precluded because data for $S(Q)$ and $g(r)$ are not available for their special conditions of density and temperature.

In the collective regime for $0.8 \leq Q \leq 4.0$ Å^{-1} neither the screened-response-function theory of Kerr and Singwi nor the present memory-function theory gives a satisfactory description of experiment. The Kerr-Singwi theory has too broad a quasielastic response, which appears to overdamp the excitations that give rise to the inelastic wing. The memory-function theory has too little damping and predicts a peak at finite frequency. At the smallest wave vectors, however, the memory-function theory is more satisfactory, as is expected from its consistency with hydrodynamics. Neither theory has any adjustable parameters and a relaxation of this strict requirement or use of improved structural data might well bring both theories into agreement with experiment. It is known, for example, that the form of the response is very sensitive to the form of $g(r)$ for r just less than the nearest-neighbor distance.

In the single-particle regime, $4 < Q \leq 12.5$ Å^{-1}, the scattered distribution moves off the frequency axis; at large Q its frequency tends to the recoil frequency $\hbar Q^2/4\pi m$ and its width becomes proportional to Q. Superimposed on this general behavior are oscillations in the peak height, width, and frequency that persist to wave vectors as large as 8 Å^{-1}. The oscillations are such that a maximum in peak height is accompanied by minima in width and frequency and by an asymmetry in the form of a high-frequency tail. The Kerr-Singwi theory is in reasonable agreement with experiment for $Q \lesssim 7$ Å^{-1} but at larger wave vectors predicts a width that is too large and a frequency that is too small. The Gram-Charlier theory evaluated for neon in this paper is in good agreement with experiment throughout the single-particle regime with an rms error about half that of the Kerr-Singwi theory. Both theories are consistent with the suggestion that the oscillations, which are similar to those observed in liquid helium, are a result of coherent interference effects that are a general property of liquids and should occur also in solids in a modified form.

ACKNOWLEDGMENTS

The authors thank Dr. W. C. Kerr for sending us the detailed results of his calculations for liquid neon. The technical assistance of R. S. Campbell is gratefully acknowledged.

---

*Now at Universidad Autonoma, Campo de Ixtapalapa, México, D.F.

[1]K. Sköld, J. M. Rowe, G. Ostrowski, and P. D. Randolph, Phys. Rev. A 6, 1107 (1972).

[2]J. M. Rowe and K. Sköld, in *Neutron Inelastic Scattering*, (International Atomic Energy Agency, Vienna, 1972), p. 413.

[3]R. A. Cowley and A. D. B. Woods, Can. J. Phys. 49, 177 (1971).

[4]Inelastic peaks have also recently been observed in coherent neutron-scattering data for liquid parahydrogen by K. Carneiro, M. Nielsen, and J. P. McTague [Phys. Rev. Lett. 30, 481 (1973)].

[5]J. R. Stehn, M. D. Goldberg, B. A. Magurno, and R. Wiener-Chasman, Neutron Cross Sections, Brookhaven National Laboratory Publ. No. BNL 325, 2nd ed., Suppl. 2, 1964 (unpublished).

[6]J. O. Hirschfelder, C. F. Curtiss, and R. B. Bird, *Molecular Theory of Gases and Liquids* (Wiley, New York, 1954).

[7]For a preliminary account of these experiments see W. J. L. Buyers, V. F. Sears, P. A. Lonngi, and D. A. Lonngi, in Ref. 2, p. 399. A complete listing of the present data for $S(Q, \nu)$ can be found in Atomic Energy of Canada Ltd. Publ. No. AECL-4910, Chalk River, Ont., 1974.

[8]It will sometimes be convenient to denote the scattering function as $S(Q, \omega)$, where $\omega = 2\pi\nu$ is the energy transfer in units of $\hbar$. In either case the normalization is chosen such that the static structure factor is given by $S(Q) = \int_{-\infty}^{\infty} S(Q, \nu)\, d\nu = \int_{-\infty}^{\infty} S(Q, \omega)\, d\omega$.

[9]The Ge monochromator was used only for the experiments with the smallest values of E ($E = 3.040$ THz), where the higher-order components are appreciable. It eliminates the second-order neutrons. Third-order neutrons and second- and higher-order neutrons in the experiments at large values of E contribute a negligible amount to the distortion of $S(Q, \nu)$.

[10]By intensity we mean the count rate per unit monitor count rate after background subtraction. The relation between the intensity and the scattering function is discussed in Sec. III.

[11]L. Van Hove, Phys. Rev. 95, 249 (1954).

[12]V. F. Sears, Adv. Phys. (to be published).

[13]L. P. Kadanoff and P. C. Martin, Ann. Phys. (N.Y.) 24, 419 (1963).

[14]V. F. Sears, Can. J. Phys. 47, 199 (1969).

[15]V. F. Sears, Can. J. Phys. 48, 616 (1970).

[16]R. D. Mountain, Rev. Mod. Phys. 38, 205 (1966).

[17]C. Gladun, Cryogenics 6, 27 (1966).

[18]P. A. Fleury and J. P. Boon, Phys. Rev. 186, 244 (1969).

[19]E. Löchtermann, Cryogenics 3, 44 (1963).

[20]F. Huth, Cryogenics 2, 368 (1962).

[21]Since, to our knowledge, the bulk viscosity of liquid neon has not been measured we use a value obtained from the law of corresponding states (Ref.6) according to which the ratio ζ/η has the same value (apart from quantum effects) in liquid neon as in liquid argon at the same reduced temperature. Ultrasonic attenuation measurements in liquid argon [D. G. Naugle, J. Chem. Phys. 44, 741 (1966)] give $\zeta/\eta = 0.69$ at 90 °K, which corresponds to $T^* = 0.756$.

[22]C. H. Chung and S. Yip, Phys. Rev. 182, 323 (1969).

[23]L. Verlet, Phys. Rev. 159, 98 (1967).

[24]L. Verlet, Phys. Rev. 165, 201 (1968).

[25]D. Stirpe and C. W. Tompson, J. Chem. Phys. 36, 392 (1962); see also P. W. Schmidt and C. W. Tompson, in *Simple Dense Fluids*, edited by H. L. Frisch and Z. W. Salsburg (Academic, New York, 1968), p. 38.

[26]P. G. de Gennes, Physica 25, 825 (1959).

[27]H. G. Bell, A. Kollmar, B. Alefeld, and T. Springer, Phys. Lett. 45A, 479 (1973).

[28]J. R. D. Copley and J. M. Rowe, Phys. Rev. Lett. 32, 49 (1974).

[29]K. S. Singwi and A. Sjölander, Phys. Rev. 120, 1093 (1960).

[30]V. F. Sears, Phys. Rev. 185, 200 (1969).

[31]V. F. Sears, Phys. Rev. A 7, 340 (1973).

[32]L. D. Landau and E. M. Lifshitz, *Statistical Physics* (Addison-Wesley, Reading, Mass., 1958), p. 102.

[33]V. F. Sears, Phys. Rev. A 1, 1699 (1970).

[34]V. F. Sears, Ber. Bunsenges. 75, 376 (1971).

[35]V. F. Sears, Phys. Rev. A 5, 452 (1972).

[36]W. C. Kerr and K. S. Singwi, Phys. Rev. A 7, 1043 (1973).

[37]S. H. Chen, O. J. Eder, P. A. Egelstaff, B. C. G. Haywood, and F. J. Webb, Phys. Lett. 19, 269 (1965).

[38]D. G. Henshaw, Phys. Rev. 111, 1470 (1958).

[39]L. A. de Graaf and B. Mozer, J. Chem. Phys. 55, 4967 (1971).

[40]R. A. Cowley, Atomic Energy of Canada Ltd. Publ. No. AECL 3189, Chalk River, Ont., 1968.

[41]See, e.g., G. Dolling and V. F. Sears, Nucl. Instrum. Meth. 106, 419 (1973).